Molecular Dynamics Assignment of NMR Correlation Times to Specific Motions in a "Basket-Handle Porphyrin" Heme

Razvan Popescu,[†] Joël Mispelter,[†] Jacques Gallay,[‡] and Liliane Mouawad*[,†]

Laboratoire de Biophysique Moléculaire, Institut Curie, Université Paris-Sud, Bât. 112, 91405 Orsay Cedex, France, and Laboratoire pour l'Utilisation du Rayonnement Electromagnétique (LURE), Université Paris-Sud, Bât. 209D, 91405 Orsay Cedex, France

Received: July 29, 2004; In Final Form: November 30, 2004

Iron (II) basket-handle porphyrins (BHP) are a series of encumbered heme models designed several years ago to mimic the ligand binding site of hemoproteins. Contrary to expectations, kinetic investigations have revealed that the k_{on} rates for CO and/or O_2 binding were only marginally affected by the assumed central steric hindrance of the iron atom. Thus, it was hypothesized that the internal dynamics of the molecule might be at the origin of the poor steric protection. To address this issue, measurements of nuclear magnetic resonance relaxation rates, fluorescence anisotropy experiments, and molecular dynamics simulations were undertaken. The size of BHP is small enough to allow the simulation in explicit chloroform with an almost complete sampling of the conformational space. The order parameters calculated from the MD trajectory compare well with the NMR experimental data and the predicted rotational correlation time corresponding to the Brownian motion of the molecule is in good agreement with the fluorescence measurements. Moreover, combining the results obtained using the three techniques allows the attribution of each internal NMR correlation time to a particular internal motion, revealing that even such medium-sized molecules are able to display quite complex internal dynamics. In particular, the handle phenyls that were assumed to sandwich the porphyrin have in fact a vanishing probability to be found in the proximity of the iron atom. They are therefore unable to reduce ligand accessibility significantly, which may explain the behavior of the k_{on} rates.

Introduction

The function of hemoproteins in oxygen storage and transport (myoglobin and hemoglobin), in enzymatic reactions (cytochromes) or in the interaction of metalloporphyrins with nitrogen oxide is intimately associated with their heme environment. To investigate their structure−function relations in detail, dozens of biomimetic heme models were chemically engineered[1−9] and more particularly those based on the "picket fence porphyrin" model.[10] In this global approach, that has been sometimes compared to a "*chemical equivalent of site directed mutagenesis*",[11] three major goals were considered: (i) to achieve pentacoordination of the heme in order to mimic the "deoxy" forms of the proteins; (ii) to reproduce the binding affinity and kinetics of O_2 and CO, in particular reducing CO affinity (the so-called discrimination problem); (iii) to avoid auto-oxidation. These issues were addressed by building chemically adjustable "superstructures" anchored on the heme macrocyle, to control locally the (proximal) pentacoordination of the heme with a nitrogeneous base on one hand and the (distal) steric hindrance and polarity on the other hand (see refs 2 and 12 for state of the art reviews).

The "basket-handle porphyrins" (BHP) are versatile series (Figure 1A). Generally, the "handles" are anchored to the *meso*-phenyls of the tetraphenyl porphyrin core by means of either an amide group, as here, or an ether group;[13−16] their lengths are adjustable. One of the handle phenyls can be replaced by a nitrogenous hanging base (pyridine, imidazole) to provide pentacoordination,[17] mimicking the proximal side of the porphyrin. On the other side, it is expected that the replacement of the ether by an amide linkage would introduce larger handle rigidity, which would increase significantly the crowding of the distal face by the phenyl group.

Kinetic and thermodynamic investigations of the binding of ligands like CO or O_2 with five-coordinated Fe^{II} heme models encumbered on their distal side showed that the ligand must overcome two free energy barriers sequentially:[18,19] the internal reaction barrier, which is analogous to what is encountered in simple "heme models", and the outer barrier, which is due to the steric hindrance caused by the distal environment. However, the comparison of whole families of related heme models using linear free energy relationships (LFER) showed that, as expected, a moderate steric crowding modulates the affinity for ligands by predominantly affecting the "off" rate, but surprisingly, it exerts little effect upon the "on" rate.[20−22] This rather disappointing result is illustrated in Figure 1B for the BHP family. Obviously, in the unliganded form the distal handle does not adopt a simple central hindrance conformation and must be either distorted or undergoing significant lateral displacements.

To verify this hypothesis NMR experiments were undertaken on the unliganded state of one molecule of the BHP family, a cross-trans-linked tetraphenylporphyrin in which the NH−CO−$(CH_2)_2$−C_6H_4−$(CH_2)_2$−CO−NH handles bind two opposite *meso*-phenyl groups[23−26] (conformation shown in Figure 1A). This molecule was chosen because it has less tendency for aggregation than the other molecules of the series. Moreover, since it is symmetrical, it is more appropriate for NMR relaxation experiments in ^{13}C natural abundance, which is preferable to avoid cross relaxation between adjacent ^{13}C atoms.

* Corresponding author. E-mail: liliane.mouawad@curie.u-psud.fr. Telephone: +33 (0)1 69 86 71 51. Fax: +33 (0)1 69 07 53 27.

[†] Laboratoire de Biophysique Moléculaire, Institut Curie, Université Paris-Sud.

[‡] Laboratoire pour l'Utilisation du Rayonnement Electromagnétique (LURE), Université Paris-Sud.

10.1021/jp046609u CCC: $30.25
Published on Web 01/29/2005

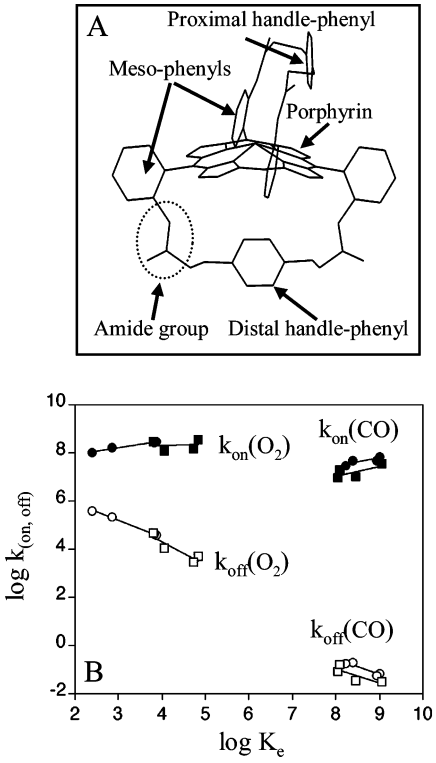

Figure 1. (A) Constructed structure of one molecule of the BHP family, a cross-trans-linked tetraphenylporphyrin. The submolecular elements are indicated, i.e., the porphyrin, the *meso*-phenyls, and the distal and proximal handle phenyls. The hydrogen atoms are not drawn. Although the iron atom is tetracoordinated, the porphyrin is artificially domed as in pentacoordinated species. (B) Partial linear free energy relation (LFER): plot of the "on" and "off" rates for "hanging base" BHP molecules binding with oxygen and carbon monoxide vs the equilibrium constant $K_e = k_{on}/k_{off}$. In these molecules, the proximal handle incorporated a pyridine that provided pentacoordination of the porphyrin. The distal handle incorporated either an ether linkage (circles) or an amide linkage (squares) and, in the order of decreasing affinity, it consisted of C_{12} aliphatic chain, C_{10} aliphatic chain, C_4-phenyl$-C_4$, and C_3-phenyl$-C_3$ (corresponding to the molecule studied here). Variations of affinity essentially result from changes of the "off" rates with only small variations of the "on" rates.

Although the chosen BHP does not contain a hanging base on its proximal side, it remains a good candidate for the study of the distal side dynamics in the BHP family.

Molecular dynamics (MD) simulations were undertaken in parallel to compare with NMR data and give a detailed description of the internal motions of BHP. Indeed in the study of such a medium-sized molecule the conformational space is expected to be sampled almost completely.

Finally, fluorescence anisotropy decay experiments were performed in order to obtain precise information concerning the global motion of the molecule, which is necessary for the NMR data interpretation.

Materials and Methods

To study experimentally the dynamics of BHP we used a symmetrical tetracoordinated species (corresponding to unbound heme) with planar porphyrin. However to avoid the iron's paramagnetic effects in NMR relaxation rate measurements, the metal was replaced by a zinc atom, assuming that the dynamics of the handles will not be affected. For comparison, the same species was used in fluorescence experiments. On the contrary, in MD simulations, it was more interesting to break the symmetry in order to gain more insight into the dynamics of a

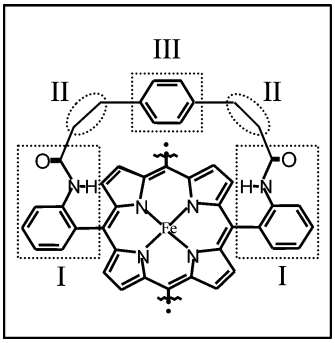

Figure 2. 2D representation of BHP. For the sake of clarity, only one handle is presented. The partition used for determining the MD parameters is shown by dashed lines.

pentacoordinated BHP (the state corresponding to a singly liganded heme). Thus, an artificially domed iron prophyrin was used in the simulations (as shown in Figure 1A).

1. Molecular Dynamics Simulations. No X-ray diffraction or NMR structure of BHP is available. We therefore constructed the (Fe)BHP molecule by using the known crystal structure of a closely similar synthetic heme model, the so-called "hybrid model",[26] which has two "pickets" like the "picket-fence" model[10,12,27,28] and one aliphatic handle on the same side of the porphyrin.

The molecular dynamics simulations of (Fe)BHP were carried out in a chloroform solution (the solvent used in the NMR experiments) including explicitly all hydrogen atoms which were added using the HBUILD facility[29] in the CHARMM program.[30]

1.1. Force Field Parametrization. The parameters for BHP were constructed as follows: for the first part of the handle consisting of the *meso*-phenyl and the amide group (Figure 2) the parameters were those of acetanilide described by Hayward et al.;[31] for the second part of the handle (CH_2-CH_2) they were taken from those of the central part of a butane chain;[32] the parameters of the handle phenyls (the phenyls that are in the center of the handles) were adjusted from the CHARMM parameter set 24 for the aromatic ring of a phenylalanine with explicit hydrogens; for the *meso*-phenyls, i.e., the phenyls attached to the meso carbons of the prophryrin, the force constant characterizing the dihedral angle around the bond between the phenyl and the porphyrin was adjusted to yield the same quantum mechanical energy barriers as those calculated by Tsuzuki and Tanabe[33] for the biphenyl molecule. Finally, for the Fe−porphyrin, the pentacoordinated-iron heme parameter set of CHARMM 24, corresponding to the domed conformation, was used, even though our model is a tetracoordinate Zn conformation. As mentioned above, this choice was made in order to break the symmetry of the molecule and to simulate the state corresponding to a singly liganded porphyrin. At the junction of all the different parts of the molecule, the partial charges were adjusted using the Mulliken method with a B3LYP/6-31G* basis in program Gaussian.[34] Concerning the solvent, the chloroform parameters were taken from Tironi and van Gunsteren.[35]

The nonbonded interactions were truncated to zero by applying the function switch of CHARMM between 8 and 12 Å, and the dielectric constant was equal to 2 (for a nonpolar solvent).

1.2. The Procedure. 1.2.1. BHP in a Vacuum. The energy of BHP was first minimized in a vacuum by the steepest descent (SD) method for 1000 steps, followed by the adopted basis Newton−Raphson (ABNR) method for 4000 steps, until the potential energy gradient was smaller than 10^{-5} kcal/mol·Å. In

the following, the length of the bonds involving hydrogen atoms were constrained with the SHAKE algorithm[36] and Newton's equations of motion were integrated using the Verlet algorithm[37] with an integration step of 2 fs. The structure of BHP was almost spherical; its dimensions along its principal axes were: 13.14, 12.97, and 12.29 Å.

1.2.2. Solvent Box. A cubic box filled with 1000 chloroform molecules was created to accommodate BHP. The box dimensions (51.06 Å)^3 were chosen in order to ensure that the minimum distance between BHP and the edge of the box was larger than 15.32 Å, i.e., three chloroform molecules. The solvent was first heated to 300 K for 40 ps and then equilibrated at 300 K for 40 ps, using the periodic boundary conditions. Finally its energy was minimized using the SD method, for 3000 steps, followed by ABNR for 1000 steps, until the gradient of the potential energy was smaller than 10^{-5} kcal/mol·Å. The energy was minimized to bring the solvent to a temperature comparable to that of BHP, i.e., around 0 K.

1.2.3. Solvated BHP. Upon insertion of BHP in the solvent box, a set of 26 chloroform molecules within a distance of 3 Å around the BHP atoms were removed. The partial density of the remaining chloroform molecules was then corrected (at 300 K, the chloroform density solution is 1.49 g/cm^3), by adjusting the box edge dimension from 51.06 to 50.63 Å. Finally, the box consisted of 974 chloroform molecules, so that the total system was composed of 5003 atoms, 133 of which belonging to the BHP molecule.

The energy of the solvated BHP was minimized as follows: first, the solvent's was minimized keeping BHP fixed, then BHP was energy minimized keeping the solvent fixed and finally, the whole system (BHP + solvent) was energy minimized without any constraints.

An MD trajectory was generated using periodic boundary conditions to remove spurious edge effects. The system was heated by 1 K increments from 0 to 300 K during 60 ps and subsequently equilibrated for 40 ps at 300 K. Then a 10 ns trajectory was generated. The total energy (kinetic + potential) was 504.8 ± 1.2 kcal/mol, and the average temperature was 302 ± 2.4 K.

2. NMR Experiments. *2.1. NMR ^{13}C Relaxation Spectroscopy.* Heteronuclear $^1H-^{13}C$ experiments were carried out at 295 K using two different spectrometers, Bruker Advance 300 and Varian Unity 500, equipped with a pulsed field gradient and a triple resonance probe. Therefore, the NMR experiments were performed at two different magnetic fields, 7.05 and 11.744 T, corresponding to 300 and 500 MHz, respectively. The experimental longitudinal and transversal relaxation rates, R_1 and R_2, were acquired with spectral widths of 5500 and 4000 Hz in the ^1H and ^{13}C dimensions, respectively. The ^1H carrier was placed on the residual HDO resonance (4.74 ppm) and the ^{13}C carrier was set at 55 ppm. All spectra were acquired in the phase-sensitivity mode by using quadrature detection in the ω_1 dimension. The pulse sequence used was described by Mispelter et al.[38]

2.2. Sample Preparation for NMR. (Zn)BHP was synthesized and purified in our laboratory.[23] The iron atom was replaced by Zn in order to suppress any paramagnetic effects of the metal. NMR measurements were performed in degassed chloroform solution sealed under argon atmosphere. The spectra being recorded at natural ^{13}C isotope abundance, the BHP samples' concentration was 10 mM, to improve the signal-to-noise ratio.

3. Fluorescence Anisotropy Decay Experiments. The fluorescence of (Zn)BHP in chloroform solution was measured using a laser diode previously described by Vincent et al.[39] The detector was a Hamamatsu model H3460-53, with a time resolution of ~11 ps. The Zn−prophyrin was excited at λ_{ex} = 428 nm and the fluorescence measured at λ_{em} = 610 nm. The sample's concentration corresponded to an OD ≈ 2 and the temperature was 291 K. Analysis of the fluorescence intensity and anisotropy decays, as a sum of exponentials, was performed according to the maximum entropy method.[40]

Results

Comparison between NMR data and MD simulations requires the previous knowledge of the global rotational correlation time (τ_R) of BHP in chloroform. Therefore, τ_R was calculated using the several techniques described in Materials and Methods, but first the Stokes−Einstein equation was used for a rough estimation of this value.

1. Rotational Correlation Time. *1.1. Calculation from the Stokes−Einstein Equation.* Because BHP is almost spherical (see Materials and Methods), τ_R was first roughly estimated using the Stokes−Einstein formula for a spherical Brownian particle:

$$\tau_R = \frac{\eta V}{k_B T} = \frac{1}{6D_R} \tag{1}$$

where V is the particle's volume, η, the solvent's viscosity, T, the system temperature, k_B, Boltzmann's constant and D_R, the rotational diffusion coefficient.

Contrary to the case of proteins, the volume estimation of BHP does not require inclusion of the first hydration shell, since no hydrogen-bonds are involved in the interactions of the molecule with chloroform.

To calculate the volume of BHP, the average structure along the 10 ns trajectory was energy minimized and its volume determined using the CHARMM program: V = 1154 Å^3 (or R ≈ 6.456 Å) showing no important modifications of the dimensions of BHP since it is comparable to the dimensions calculated for the initial structure (see Materials and Methods). This yields, at the average temperature of the simulation (302 K), τ_R = 143.9 ps and $D_R = 1.16 \times 10^9$ s^{-1}.

1.2. Calculation from the MD Trajectory. The translational and rotational correlation times can be calculated from the MD trajectory using the differential laws of the Brownian motion given by Einstein's equations:

$$\langle \Delta r^2 \rangle = 6D_T \Delta t \tag{2}$$

$$\langle \Delta \theta^2 \rangle = 4D_R \Delta t = \frac{2}{3}\frac{\Delta t}{\tau_R} \tag{3}$$

where Δr is the infinitesimal distance by which the center of mass moves and $\Delta\theta$ the angle by which a molecule-bound fixed vector rotates during the time interval Δt; brackets correspond usually to ensemble averages, but here they refer to time averages since, according to the ergodic theorem, ensemble and time averages are interchangeable. Equations 2 and 3 define the translational and rotational diffusion coefficients, D_T and D_R, respectively. However, the differential law for rotational diffusion being appropriate for only short-time displacements, it is more convenient to use the integrated form of this diffusion for a long trajectory as here. In this form, the rotational diffusion law for a spherical Brownian particle is given by[41]

$$\left\langle \frac{3\cos^2\theta(t) - 1}{2} \right\rangle = \exp(-6D_R t) = \exp(-t/\tau_R) \tag{4}$$

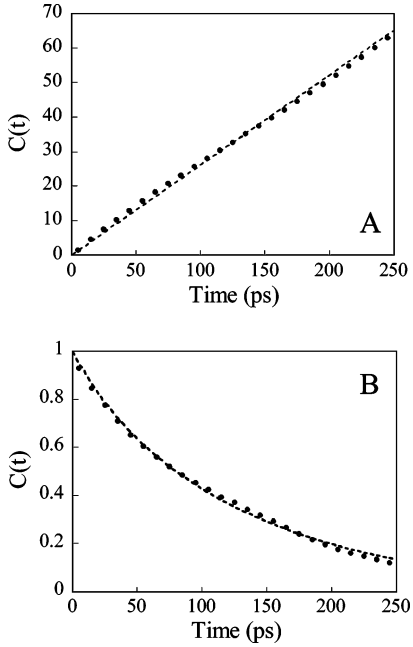

Figure 3. Correlation function for the translation (A) and rotation (B) of BHP in chloroform calculated from the MD trajectory (filled circles) and fitted using eq 2 and 4, respectively (dashed lines). Only 2% of the data points are plotted.

This also corresponds to the autocorrelation function, $C_{AB}(t)$ of a vector AB attached to the Brownian particle. It can be computed from the MD trajectory using the equation:[42,43]

$$C_{AB}(t) = \langle P_2(\cos\theta_{AB})\rangle = \left\langle \frac{3\cos^2\theta_{AB}(t) - 1}{2} \right\rangle = \frac{1}{T_{MD} - t}\sum_{t'=0}^{T_{MD}-t} \frac{3[\hat{\mu}_{AB}(t')\cdot\hat{\mu}_{AB}(t'+t)]^2 - 1}{2} \quad (5)$$

where $P_2(\cos\theta_{AB})$ is the second rank Legendre polynomial, $\hat{\mu}_{AB}$, the unit vector along the AB direction (here AB is one of the principal axes of BHP that is parallel and close to the porphyrin's plane), θ_{AB}, the AB vector rotational angle, T_{MD}, the total time of the MD trajectory (in this work 10 ns), and t', the time corresponding to each MD frame running from 1 to $T_{MD} - t$ (t maximum does not exceed $T_{MD}/10$ to ensure good statistics).

As predicted in eqs 2 and 4, the differential translational diffusion curve is linear and the integral rotational diffusion is monoexponential (Figure 3). The fits of these curves yield $D_T = 4.3 \times 10^{-6}$ cm^2 s^{-1} and $\tau_R = 119.5$ ps corresponding to $D_R = 1.39 \times 10^9$ s^{-1}.

1.3. Calculation from Fluorescence Experiments. The fluorescence anisotropy $R(t)$ is defined by:

$$R(t) = \frac{I_{vv}(t) - I_{vh}(t)}{I_{vv}(t) + 2I_{vh}(t)} = R(0)\left\langle \frac{3\cos^2\theta(t) - 1}{2} \right\rangle = R(0)\exp(-t/\tau_R) \quad (6)$$

in which $I_{vv}(t)$ and $I_{vh}(t)$ are the polarized fluorescence intensities. The first and the second subscripts refer to the orientation of the excitation and emission polarizers, respectively. v corresponds to vertical and h to horizontal directions.

The three independent measurements performed with the laser diode yielded $\tau_R = 133 \pm 13$, 137 ± 4, and 170 ± 8 ps.

1.4. Calculation from NMR Experiments. In the NMR experiments, the BHP molecule cannot be considered as a Brownian particle because what we measure are the relaxation rates of its C−H bonds. Thus, internal motions should be taken into account. For this purpose, the dipolar relaxation between two nuclei α and β in solution is considered instead of the AB vector mentioned above that corresponded to the principal axis of the molecule. It is generally assumed that the relaxation due to the molecule overall rotation is decoupled from the relaxation due to its internal dynamics,[44] thus the time correlation function, $C_{\alpha\beta}(t)$, that describes the orientation of the inter-nuclei vector $\alpha\beta$ can be factorized as

$$C_{\alpha\beta}(t) = (^1/_5)C_O(t)C_I(t) \quad (7)$$

where $C_O(t)$ and $C_I(t)$ correspond to the correlation functions of the overall rotational tumbling and to that of the internal dynamics, respectively. According to eqs 4 and 5, $C_O(t) = e^{-t/\tau_R}$.

2. Internal Motions. *2.1. NMR Models.* In the internal correlation function, $C_I(t)$, the $\alpha\beta$ vector corresponds to any two atoms used in the NMR measurements; in the case of BHP, this vector corresponds to a C−H bond:

$$C_I(t) = \langle P_2(\cos\theta_{CH})\rangle = \langle P_2(\hat{\mu}_{CH}(0)\cdot\hat{\mu}_{CH}(t))\rangle \quad (8)$$

where $\hat{\mu}_{CH}$ is the unit vector along the C−H bond direction expressed in the internal reference frame of the molecule. However, what is determined experimentally are the longitudinal and transversal relaxation rates, R_1 and R_2, that are related to molecular motions through the spectral density function, $J(\omega)$:

$$R_1^{\nu_s} = \frac{d_C^2}{4}[J(\omega_H - \omega_C) + 3J(\omega_C) + 6J(\omega_C + \omega_H)] + \frac{1}{3}(\Delta_C^{CSA})^2\omega_C^2 J(\omega_C) \quad (9)$$

$$R_2^{\nu_s} = \frac{d_C^2}{8}[4J(0) + J(\omega_H - \omega_C) + 3J(\omega_C) + 6J(\omega_H) + 6J(\omega_C + \omega_H)] + \frac{1}{18}(\Delta_C^{CSA})^2\omega_C^2[4J(0) + 3J(\omega_C)] + R_{ex} \quad (10)$$

where ω_C and ω_H are ^{13}C and ^{1}H Larmor pulsations corresponding to each spectrometer frequency ($\nu_s = 300$ or 500 MHz), $d_C = 1.46 \times 10^5$ s^{-1} the dipolar interaction for the C−H bond and $\Delta_C^{CSA} = \sigma_{\parallel} - \sigma_{\perp}$ is the chemical shift anisotropy (CSA) defined as the difference between the parallel and the perpendicular components of the ^{13}C chemical shift tensor, $\boldsymbol{\sigma}$. The components of $\boldsymbol{\sigma}$ in the case of aromatic, polyaromatic and macrocycles including nitrogen (pyridine, pyracene, pyrrols, ...) are on the same order of magnitude[45−49] and lead to $\Delta_C^{CSA} \approx -180$ ppm. R_{ex} corresponds to the chemical exchange contribution to the transversal relaxation rate. $J(\omega)$ is the Fourier transform of the correlation function, $C_I(t)$.

Depending on the complexity of the internal motion, $C_I(t)$ can be approximated by either a monoexponential or a biexponential function, according to the Lipari−Szabo and the Clore−Szabo models, respectively.

2.1.1. The Lipari−Szabo "Model-Free" Approach. In this model,[50] the internal correlation function is monoexponential, describing simple motions that take place on one time scale:

$$C_I(t) = S^2 + (1 - S^2)e^{-t/\tau_e} \quad (11)$$

where τ_e is an internal effective correlation time, and S^2 the generalized order parameter which is calculated from the limiting value of $C_I(t)$:

$$S^2 = \lim_{t\to\infty} C_I(t) = \lim_{t\to\infty} \langle P_2(\hat{\mu}_{CH}(0)\cdot\hat{\mu}_{CH}(t))\rangle \qquad (12)$$

Thus, $J(\omega)$ is expressed as follows:

$$J(\omega) = \frac{2}{5}\left[\frac{S^2\tau_R}{1+(\omega\tau_R)^2} + \frac{(1-S^2)\tau'_e}{1+(\omega\tau'_e)^2}\right] \qquad (13)$$

where $\tau'_e = \tau_e\tau_R/(\tau_e + \tau_R)$.

2.1.2. The Clore−Szabo Extended Model. To describe more complex motions that may take place on two time scales, an "extended model" has been developed by fitting the internal correlation function to a double exponential:[51]

$$C_I(t) = S^2 + (1 - S_{fast}{}^2)e^{-t/\tau_{fast}} + (S_{fast}{}^2 - S^2)e^{-t/\tau_{slow}} \qquad (14)$$

where $S_{fast}{}^2$ is an additional order parameter characterizing the short time scale motion, and τ_{fast} and τ_{slow} are correlation times describing the fast and slow decay of the internal correlation function. The fast decay is characteristic of small fluctuations in the local nuclear environment, while the slow decay describes lower frequency and larger scale motions. In this model, the spectral density function is

$$J(\omega) = \frac{2}{5}\left[\frac{S^2\tau_R}{1+(\omega\tau_R)^2} + \frac{(1-S_{fast}{}^2)\tau'_{fast}}{1+(\omega\tau'_{fast})^2} + \frac{(S_{fast}{}^2 - S^2)\tau'_{slow}}{1+(\omega\tau'_{slow})^2}\right] \qquad (15)$$

where $\tau'_i = \tau_i\tau_R/(\tau_i + \tau_R)$, i = *fast* or *slow*, and $S^2 = S_{slow}{}^2S_{fast}{}^2$.

Our aim was to derive the rotational correlation time, τ_R, but also other order parameters and correlation times for the C−H bonds of either the porphyrin or the handle phenyls. However, in the case of BHP, the number of unknowns in these models is higher than the number of experimental observables (the relaxation rates R_1 and R_2 for the prophyrin and the handle phenyls at two distinct spectrometer frequencies). Thus, one should take into account the relative rigidity of some parts of BHP to introduce more approximations and simplify the problem. For this purpose it was useful to calculate beforehand the atomic fluctuations from the MD trajectory.

2.2. Atomic Fluctuations. The atomic fluctuations, over the 10 ns trajectory (Figure 4), were calculated after reorienting the molecule of each trajectory's frame (at time t) on its original position ($t = 0$) in order to remove overall rotations and translations. They show that the porphyrin is almost rigid compared to the handles; the maximum fluctuations of its heavy atoms is 0.81 Å, while those of the handles are 1.67 and 1.91 Å, these maxima being reached for the handle phenyls (the fluctuations of the hydrogen atoms can be as large as 2.5 Å). Both handles present similar fluctuation profiles, although a slight dissymmetry is observed due to the out-of-plane position of the Fe atom in these simulations. Using the common terminology for heme proteins, the side of the porphyrin where the iron atom goes out of the plane will be called the proximal side, and by opposition, the other one will be the distal side. The proximal handle is somewhat more constrained in its movements than the distal one.

2.3. The Porphyrin Order Parameters. 2.3.1. NMR Experiments. The experimental ^{1}H−^{13}C relaxation rates, R_1 and R_2, at the two distinct spectrometer frequencies are presented in Table 1.

For the porphyrin, the longitudinal relaxation rate values, R_1, do not vary much with respect to υ_s considering the inherent experimental errors. On the contrary, R_2 increases significantly with the frequency, suggesting that an exchange process has to be taken into account (see below). Thus, only the three relaxation rate values, $R_1{}^{300MHz}$, $R_2{}^{300MHz}$ and $R_1{}^{500MHz}$ can be used to determine the order parameters and correlation times. On the other hand, since the porphyrin is relatively rigid (as shown in Figure 4), its internal motion is probably simple and the Lipari−Szabo model can be used (this assumption will be justified below from the MD trajectory). However, this still constitutes an undetermined problem with three unknowns (S^2, τ_e, and τ_R), due to the nonlinearity of $J(\omega)$. Taking into account the porphyrin rigidity, the dynamical behavior of its ^{1}H−^{13}C vectors is considered to be similar to that of the first principal axis of the molecule which is parallel and very close to the porphyrin's plane, thus we can assume that $\tau_e \ll \tau_R$ and S^2 is close to 1. With these approximations, the spectral density function (eq 13) reduces to

$$J(\omega) = \frac{2}{5}\left[\frac{S^2\tau_R}{1+(\omega\tau_R)^2}\right] \qquad (16)$$

Despite these simplifications, it is still not possible to determine analytically the order parameters and the rotational correlation times from the relaxation rates R_1 and R_2. However the relaxation rates can be mapped onto the (S^2, τ_R) plane, as shown by Jin et al.[52] For this, the porphyrin relaxation rates $R_1{}^{300MHz}$, $R_2{}^{300MHz}$ and $R_1{}^{500MHz}$ are calculated for couples of values (S^2,τ_R), with S^2 ranging from 0 to 1 with 0.02 step, and τ_R ranging from 0 to 400 ps with 5 ps step. Only the values corresponding to experimental relaxation rates are taken into account; thus, in Figure 5, only the contours delimiting the experimental uncertainties of the $R_1{}^{300MHz}$, $R_2{}^{300MHz}$, and $R_1{}^{500MHz}$ are represented. The possible solutions for S^2, and τ_R values should be compatible with all three NMR experiments, corresponding to the common area of the three error intervals delimited by the six contour plots. The S^2 values in this area are limited to the 0.65−1.0 interval (with an average value $S^2 = 0.825 \pm 0.175$) while τ_R can vary from 176 to 340 ps (with an average value $\tau_R = 258 \pm 82$ ps).

2.3.2. MD Trajectory. To calculate the order parameter, S^2, and the internal effective correlation time, τ_e, of the porphyrin

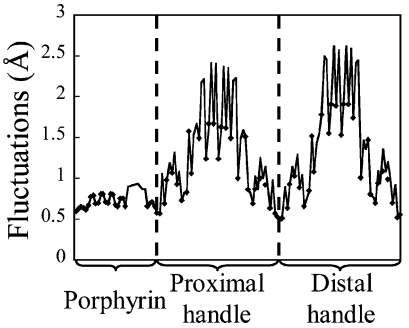

Figure 4. All atom fluctuations vs atom index calculated over the 10 ns MD trajectory. Heavy atoms are represented with circles while hydrogen atoms are represented only with lines. The highest fluctuations correspond to the phenyl group in the middle of each handle.

TABLE 1: Relaxation Rates from NMR Experiments (R_{ex} Were Calculated as Described in Subsection 3 of the Results)

	spectrometer frequency υ_s (MHz)	R_1 (s^{-1})	R_2 (s^{-1})	R_{ex} (s^{-1})
porphyrin	300	3.56 ± 0.18	3.79 ± 0.14	0.23 ± 0.32
	500	3.49 ± 0.32	6.28 ± 0.46	2.79 ± 0.78
handle phenyls	300	1.96 ± 0.10	2.10 ± 0.16	0.14 ± 0.26
	500	1.93 ± 0.14	3.64 ± 0.50	1.71 ± 0.64

TABLE 2: Relaxation Rates Calculated from the MD Trajectory for Four Values of τ_R: the Rotational Correlation Time Calculated from the MD Trajectory at the Simulation Temperature $T = 302$ K (119.5 ps) and at the NMR Experiments Temperature $T = 295$ K (132.6 ps), the Average Value Taken from the NMR Data for $S^2 = 0.9$ (206 ps), and Finally the Extreme Value from NMR Experiments (340 ps)

		R_1 (s^{-1})				R_2 (s^{-1})			
	υ_s (MHz)	$\tau_R =$ 119.5 ps	$\tau_R =$ 132.6 ps	$\tau_R =$ 206.0 ps	$\tau_R =$ 340.0 ps	$\tau_R =$ 119.5 ps	$\tau_R =$ 132.6 ps	$\tau_R =$ 206.0 ps	$\tau_R =$ 340.0 ps
porphyrin	300	2.287	2.512	3.635	5.109	2.236	2.560	3.758	5.444
	500	2.309	2.505	3.394	4.397	2.409	2.626	3.656	4.967
distal handle phenyl	300	0.932	0.987	1.231	1.505	0.943	0.999	1.253	1.551
	500	0.976	1.037	1.251	1.476	1.005	1.069	1.303	1.566
proximal handle phenyl	300	0.921	0.981	1.255	1.577	0.933	0.994	1.281	1.636
	500	0.959	1.024	1.256	1.507	0.990	1.059	1.316	1.618

from the MD trajectory the Brownian rotational and translational diffusion had to be removed first. This was done by reorienting each frame upon the mean porphyrin plane (defined by the four porphyrin's nitrogen atoms) of the minimized average BHP structure. Then the internal correlation functions, $C_I(t)$, for each of the eight C−H bonds of the porphyrin's pyrrols were calculated using eq 5 where the AB vector corresponded to the C−H bond. All eight curves had the same profile; i.e., after an ultrafast initial drop with $\tau_e = 0.1$ ps, they converged to a constant value $S^2 = 0.9$ over the whole trajectory, consistent with the monoexponential Lipari−Szabo model. These calculated values of S^2 and τ_e are in accordance with our previous assumption (S^2 close to 1 and $\tau_e \ll \tau_R$) justifying a posteriori the approximations made above in the $J(\omega)$ calculation. The value of $\tau_e = 0.1$ ps seems to be underestimated, but it corresponds well to what is usually observed in similar calculations.[53−55]

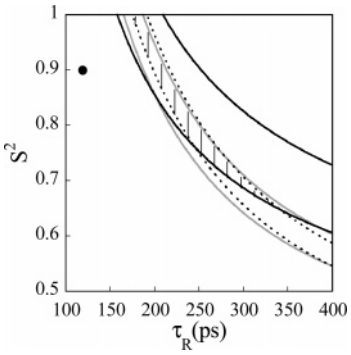

Figure 5. Porphyrin relaxation rate contours in the (S^2,τ_R) plane. The gray line contours delimit the region corresponding to R_1^{300MHz} (3.38 s^{-1} and 3.74 s^{-1}), the bold lines correspond to R_1^{500MHz} (3.17 s^{-1} and 3.81 s^{-1}) and the dotted lines to R_2^{300MHz} (3.79 s^{-1} and 3.93 s^{-1}). The hatched area represents the allowed region for (S^2,τ_R) as obtained from NMR experiments and the filled circle corresponds to the (S^2,τ_R) couple calculated from the MD trajectory.

Replacing S^2 by its value (0.9) in the above results, obtained from NMR experiments (described in Section 2.3.1 and Figure 5), yields τ_R between 199 and 213 ps, with an average value of 206 ps.

From these values, the relaxation rates R_1 and R_2 were calculated using eqs 9, 10, and 13 for several values of τ_R. Notice that in eq 10 R_{ex} was not taken into account. The results reported in Table 2 show good agreement with experimental data (Table 1) when $\tau_R = 206$ ps.

2.4. The Handle Phenyls Order Parameters. 2.4.1. NMR Experiments. As for the porphyrin, the transversal relaxation rate, R_2, varies significantly with the frequency, showing the existence of an exchange process. Thus, only the three relaxation rate values, R_1^{300MHz}, R_2^{300MHz}, and R_1^{500MHz}, can be used to determine the order parameters.

As shown by the atomic fluctuations (Figure 4), the handle phenyls are much more flexible than the porphyrin core. They are expected to undergo at least two types of internal motions, which makes the Clore−Szabo extended model more appropriate to describe them. Unfortunately, the number of unknowns

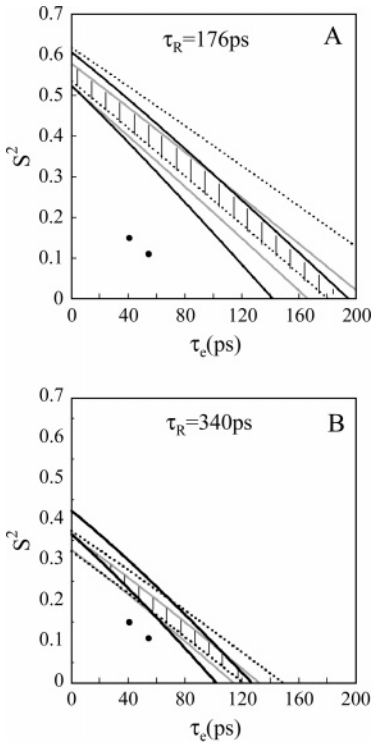

Figure 6. Handle-phenyls relaxation rates contours in the (S^2,τ_e) plane corresponding to the extreme values of the rotational correlation time, $\tau_R = 176$ ps (A) and $\tau_R = 340$ ps (B). The gray line contours delimit the region corresponding to R_1^{300MHz} (1.86 s^{-1} and 2.06 s^{-1}), the bold lines correspond to R_1^{500MHz} (1.79 s^{-1} and 2.07 s^{-1}) and the dotted lines to R_2^{300MHz} (1.94 and 2.26 s^{-1}). The hatched area represents the allowed region for (S^2,τ_e) as obtained from NMR experiments and the filled circles correspond to the (S^2,τ_e) couples for the distal and proximal handle phenyls as calculated from the MD trajectory.

in this model is larger than that of the experimental data set. Therefore, in a first approximation the Lipari−Szabo model (eq 13) will be used. As for the porphyrin, the S^2 and τ_e values cannot be determined analytically, especially as no further approximations are possible. Thus, the handle-phenyls relaxation rates R_1^{300MHz}, R_2^{300MHz}, and R_1^{500MHz} were calculated for the extreme values of τ_R found above ($\tau_R = 176$ ps and $\tau_R = 340$ ps) using couples of (S^2,τ_e) values for the phenyls, S^2 ranging from 0 to 1 with a 0.02 step, and τ_e ranging from 0 to 200 ps with a 0.1 ps step. In Figure 6, only the contours delimiting the experimental uncertainties of R_1 and R_2 are represented. The allowed solution space for (S^2,τ_e) values compatible with the

TABLE 3: Order Parameters Calculated from the MD Trajectory Using the Internal Correlation Functions for Each of the Four ^{1}H−^{13}C Vectors of the Distal (1−4) and Proximal (5−8) Handle Phenyls

phenyl C−H vectors[a]	Lipari−Szabo order parameters		Clore−Szabo order parameters				
	S^2	τ_e (ps)	S^2	$S_{slow}{}^2$	$S_{fast}{}^2$	τ_{fast} (ps)	τ_{slow} (ps)
1	0.15	39.9	0.13	0.24	0.54	5.3	116.8
2	0.15	41.1	0.13	0.24	0.54	5.4	121.0
3	0.15	40.3	0.13	0.24	0.54	5.4	117.8
4	0.15	41.4	0.13	0.24	0.54	5.3	120.7
mean	**0.15**	**40.7 ± 0.7**	**0.13**	**0.24**	**0.54**	**5.35 ± 0.05**	**119.1 ± 2.1**
5	0.11	52.2	0.09	0.14	0.64	3.1	100.2
6	0.12	56.8	0.10	0.16	0.63	3.5	116.4
7	0.11	51.2	0.09	0.14	0.64	3.1	100.0
8	0.11	56.8	0.10	0.16	0.62	3.5	117.3
mean	**0.11**	**54.2 ± 3.0**	**0.09**	**0.15**	**3.63 ± 0.01**	**3.3 ± 0.2**	**108.5 ± 9.7**

[a] Key: distal, 1−4; proximal, 5−8.

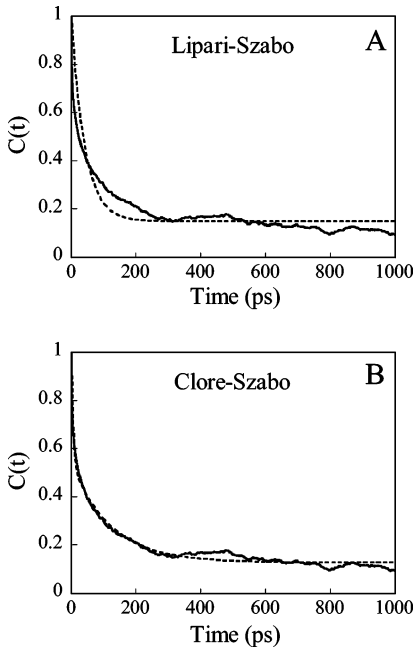

Figure 7. Internal correlation function of one ^{1}H−^{13}C vector of the handle-pyenyls (solid line). All the other vectors of both phenyls have similar profiles. The correlation function decays less rapidly than for the porphyrin; it is fitted (dashed line) using either the Lipari−Szabo model (A) or the Clore−Szabo model (B).

NMR experiments is restrained to the common area delimited by the six contour plots. For $\tau_R = 176$ ps, the S^2 values are limited to the 0−0.57 interval while τ_e can vary from 0 to 194 ps, and for $\tau_R = 340$ ps, S^2 is limited to 0−0.37 and τ_e to 0−126 ps.

2.4.2. MD Trajectory. The internal correlation functions corresponding to the four ^{1}H−^{13}C vectors of each handle phenyl were calculated from the MD trajectory (after reorienting BHP on the porphyrin's nitrogen atoms as described above) and fitted first by the Lipari−Szabo monoexponential function (eq 11). As expected, the fit was poor for both handle phenyls, because the motion of these aromatic rings is more complex than what could be described by the Lipari−Szabo model (Figure 7A). The average values for the distal phenyl are $S^2 = 0.15$ and $\tau_e = 40.7$ ps and for the proximal one, $S^2 = 0.11$ and $\tau_e = 54.2$ ps (see Table 3 for more details). These calculated couples of values (S^2,τ_e) are out of the solution area obtained from the NMR experiments (Figure 6), but they are close in the case of $\tau_R = 340$ ps.

On the contrary, the internal correlation functions were fitted more accurately (Figure 7B) by the biexponential Clore−Szabo model (eq 14). There are slight differences between the two phenyls due to the out-of-plane position of the iron atom in these simulations; they converge to slightly different values. The mean order parameters obtained from the four fits for each phenyl are reported in Table 3. From their average values, the relaxation rates were calculated using eqs 9 and 10 (without R_{ex}) for several τ_R values and were reported in Table 2.

The motion of each phenyl can be described as a combination of two different ones: the rotation around the phenyl axis and the global displacement of the phenyl accompanying the handle. Such complex motions take place on two time scales according to the Clore−Szabo extended model. Intuitively one might expect the correlation time τ_{fast} to correspond to the rotation of the phenyl with respect to its axis and τ_{slow} to the movement of the handle itself. To verify this hypothesis, the correlation time for each type of motion was calculated from the MD trajectory.

2.5. Characterization of the Handle's Global Motions. Since the most rigid part of BHP is the porphyrin's plane (defined by its four nitrogen atoms), it has been chosen as a reference frame for describing the internal dynamics of the molecule. For each MD frame, the BHP molecule was reoriented in a way that makes the nitrogen atoms' best fitted plane be approximately the *XY* reference one, with the origin at the center of mass of these atoms, the *X* axis pointing along the average position of the nitrogen atoms considered two by two (Figure 8) so that it was approximately parallel to the distal handle, and the *Y* axis pointing perpendicularly, so that it was approximately parallel to the proximal handle; in this reference system the *Z* axis points toward the reader. The center of each handle-phenyl's cycle was then projected on the *XY* plane, to represent the global movement of this aromatic ring that accompanies the handle.

These projections show that the handle's motion can be decomposed in two types: a lateral bending motion (in the direction perpendicular to the handle), and a longitudinal motion (corresponding to the sliding of the phenyl along the handle). These two movements seem to be correlated, since they result in a somehow circular motion of the phenyls that strongly avoid the central region of the porphyrin around the perpendicular to the iron.

However, a significant dissymmetry between the proximal and distal handles motion is revealed by the restricted amplitude of the proximal phenyl's sliding (the projection spans from −2.5 to +2.5 Å along the *Y*-axis corresponding to the proximal handle) compared to the distal one (±3.0 Å along the *X*-axis that corresponds to the distal handle). This is understandable because the porphyrin distortion, due to the Fe-out-of-plane position, results in the carbon-meso atoms that anchor the distal handle to point out of the porphyrin's plane toward this handle, inducing a favorable "loose" in the chain, whereas the carbon-meso atoms that anchor the proximal handle remain in the

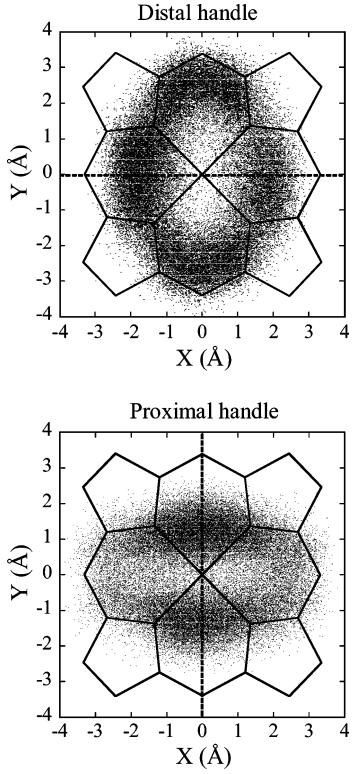

Figure 8. Projections of the centers of distal (A) and proximal (B) handle phenyls on the porphyrin plane (solid line), along the MD trajectory. The projections are represented by the black dots and the idealized directions of the handles by the dashed lines. The distal handle is oriented along the *X* axis, while the proximal one lies along the *Y* axis, the direction of the view being "above" the molecule, i.e., from the proximal side toward the porphyrin.

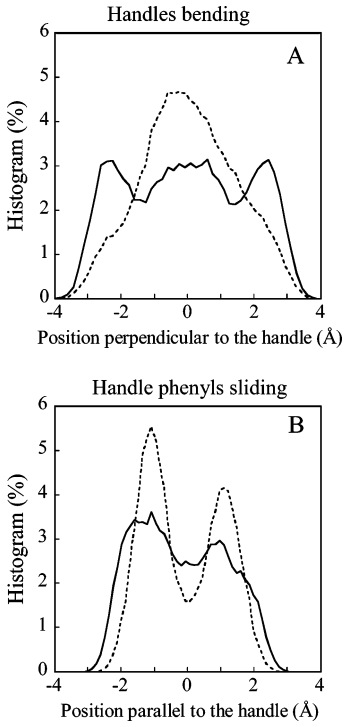

Figure 9. Histograms along *X* and *Y* axes of the projections of the distal (solid line) and proximal (dashed line) handle-phenyls centers on the plane of the porphyrin (data taken from Figure 8). They describe the probability of presence of the phenyls over one part or the other of the porphyrin, reflecting the handle's bending (A, motion along *Y* for the distal phenyl and *X* for the proximal one) and the handle's sliding (B, along *X* for the distal and *Y* for the proximal phenyls).

porphyrin's plane. In contrast, both handles present a comparable lateral bending with a maximum position (±3.8 Å along the *Y*-axis for the distal handle and the *X*-axis for the proximal one) corresponding to a bending angle of about ±40° with respect to the perpendicular to the porphyrin's plane passing through the iron atom. The most extreme populated positions of the distal handle (around ±2.5 Å) are in fact more populated than the corresponding positions of the proximal handle. These assertions can be more clearly seen in the populations histograms (Figure 9).

To calculate the transition time from one state to the other, which could be compared to the calculated values of τ_{fast} and τ_{slow}, one should first identify these states. In the histograms (Figure 9A) the bending motion does not show the presence of distinguishable states, while the phenyl's sliding motion (Figure 9B) shows the existence of two states but with an important overlap between them. Thus, for both movements, since the histograms are almost symmetrical around zero, this point was considered as the limit between two states, corresponding to the position of the phenyl above one-half or the other of the porphyrin, i.e., the negative or the positive positions along *X*- and *Y*-axes. Averaging the residence time in each state yielded for the mean lifetime: $\tau_{bending}^{distal} = 3.8$ ps, $\tau_{bending}^{proximal} = 2.4$ ps and $\tau_{sliding}^{distal} = 3.6$ ps, $\tau_{sliding}^{proximal} = 4.8$ ps. Surprisingly, these values are of the same order of magnitude as τ_{fast}.

2.6. Characterization of the Rotational Motion of the Handle Phenyls. In the same reference frame as described above, we considered the *z* position of the four central carbon atoms of the phenyl (excluding the two extreme C atoms that are also part of the handle). More precisely, the difference between the *z* coordinates of two opposing carbons was utilized to calculate

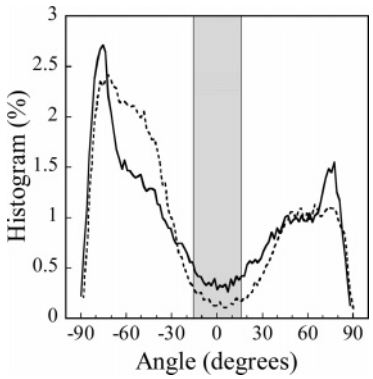

Figure 10. Histogram of the angles describing the distal (solid line) and proximal (dashed line) handle-phenyls rotation showing the presence of two distinct states. The gray strip corresponds to populations around 0° (±15°) that are difficult to precisely assign to any of the states and that are neglected in the calculation of the residence time.

the rotation angle (α) of the phenyl's plane around the axis that connects the phenyl to the handle. The porphyrin's plane was taken as reference, i.e., $\alpha = 0$ when the phenyl's plane is parallel to the porphyrin. In fact, in the calculation of the angle α the difference coordinates should be corrected in order to take into account the case where the phenyl's axis is not parallel to the porphyrin's plane; but since the corresponding error turned out to be negligible, the correction was abandoned for the sake of clarity.

The population histogram with respect to the angle α (Figure 10) shows the presence of at least two distinct states centered around zero, with very little overlap. The average residence time, $\tau_{rotation}$, can be calculated by considering the zero angle as the limit between the two states, but in the present case this would induce artifacts due to the known thermal vibrations of a phenyl

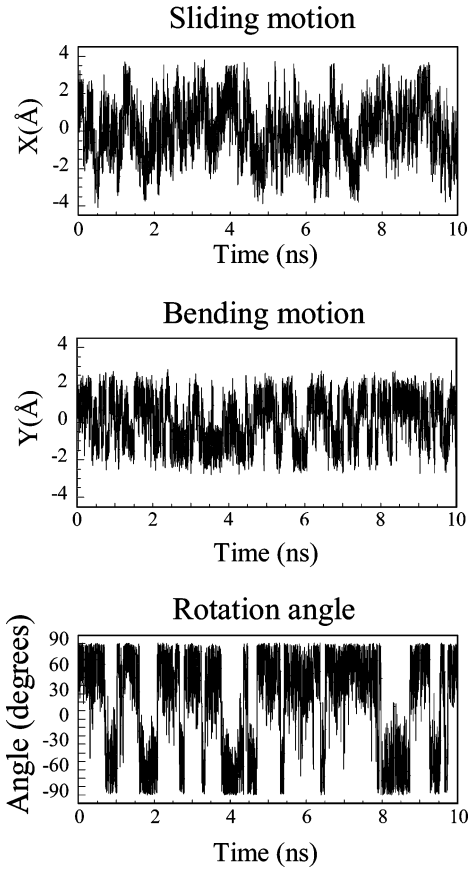

Figure 11. Position of the distal handle-phenyl center's projection on the porphyrin plane (data taken from Figure 8) vs time. The motion along the *X* axis (top) represents the sliding of the handle and along the *Y* axis (middle) represents its bending. Bottom: the rotation angle of the handle phenyl is reported with respect to time. These plots show clearly that the rotation of the phenyl is significantly slower than the motions of the handle.

of about ±15° around its average position, as found in proteins. Indeed, this would result in a very rapid transition around 0°, reflecting only the thermal vibration, not the real transition between the two distinct states. Thus, the populations between ±15° around 0° were excluded from the statistics (they corresponded to 8% of the total populations for the distal phenyl and 5% for the proximal one) yielding $\tau_{rotation}^{distal} = 39$ ps and $\tau_{rotation}^{proximal} = 82.2$ ps, almost of the same order of magnitude as τ_{slow}. If the central populations were not excluded, the calculated residence time would be slightly smaller than that considered here, but still significantly longer than the average time for bending and sliding of the handle.

This shows that, contrary to ordinary intuition, the slow motion corresponds to the rotation of the phenyl around its axis whereas the fast motion reflects the global movement of the handle. This also can be clearly seen in Figure 11, which displays the positions corresponding to these various movements vs time.

3. Exchange Process Evaluation. The calculated longitudinal and transversal relaxation rates (described above and presented in Table 2) using eqs 9 and 10 (without R_{ex}) and based on the order parameters issued from the MD trajectory are almost equal. Indeed, as can be seen in Table 2, $R_1 \simeq R_2$ for both frequencies, 300 and 500 MHz. Since R_{ex} is not included in these calculations and the relaxation rates obtained from NMR data at 300 MHz are also almost identical (Table 1), one may conclude that R_{ex} is negligible at 300 MHz. However at 500 MHz, R_2 is significantly greater than R_1 (Table 1), indicating the presence of an exchange process at this frequency. The exchange contribution to R_2 increasing with the square of the frequency, we can conclude that, at 500 MHz, R_{ex} can be approximated by the difference of NMR transversal and longitudinal relaxation rates. Using $R_{ex} \simeq R_2 - R_1$ from NMR data one obtains for the porphyrin

$$(R_{ex})^{300\text{MHz}} = 0.23 \pm 0.32\ \text{s}^{-1}$$

$$(R_{ex})^{500\text{MHz}} = 2.79 \pm 0.78\ \text{s}^{-1}$$

and for the handle phenyls

$$(R_{ex})^{300\text{MHz}} = 0.14 \pm 0.26\ \text{s}^{-1}$$

$$(R_{ex})^{500\text{MHz}} = 1.71 \pm 0.74\ \text{s}^{-1}$$

The experimental uncertainties lead to

$$0 < \frac{((R_{ex})^{300\text{MHz}})^{porp}}{((R_{ex})^{500\text{MHz}})^{porp}} < 0.37 \text{ and } 0 < \frac{((R_{ex})^{300\text{MHz}})^{phe}}{((R_{ex})^{500\text{MHz}})^{phe}} < 0.27$$

These values are close to the ratio of the squares of the spectrometer frequencies ν_s, $(300/500)^2 = 0.36$, as expected in the case of an exchange process on a time scale ranging from microseconds to milliseconds. This time scale is much larger than that of the MD simulations. However, although the calculated trajectory (10 ns) was too short for observing this exchange process, it was long enough to describe accurately all the possible internal and global motions. Moreover the calculated internal correlation times were all smaller than 120 ps, showing that this additional process cannot be explained by an exchange between any parts of BHP as it might be expected, but probably to an intermolecular exchange consequent to associations of BHP molecules in the high concentration solution used for the NMR experiments (10 mM, see Materials and Methods). This point is discussed in the next section.

Discussion

The dynamical behavior of a biomimetic molecule, BHP, was studied using several techniques. The interest of such an average-size molecule is that its overall motion can be studied easily, while it still has a relatively complex internal dynamics.

1. Rotational Correlation Time Determination. The overall tumbling of BHP in chloroform, characterized by its rotational correlation time, τ_R, was determined by theoretical (Stokes−Einstein calculations; MD simulations) and experimental techniques (fluorescence and NMR experiments). The results were obtained at different temperatures: theoretical determination at 302 K, fluorescence experiments at 291 K, and NMR at 295 K. So, to compare them, all the τ_R values were corrected to the NMR experiment temperature, taking into account the corresponding modification of the chloroform viscosity[56] (Figure 12).

What is remarkable is that not only were the MD simulations able to reproduce accurately the qualitative features of the Brownian motion theory (the rotational correlation function in the integral form being monoexponential and the translational correlation function linear as shown in Figure 3) but also their quantitative predictions turned out to be quite satisfactory compared to fluorescence experiments. This demonstrates that the chloroform force field[35] simulated well the viscosity of the solvent, which is a macroscopic property, through the microscopic nonbonded interactions (electrostatic and van der Waals). This was not usually the case for other force fields.[57]

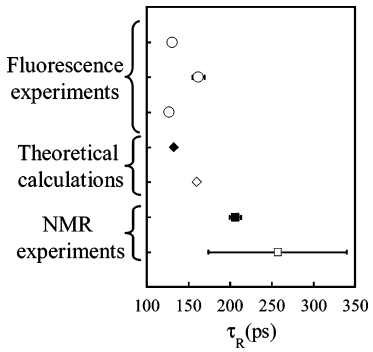

Figure 12. Rotational correlation times calculated by theoretical and experimental techniques for $T = 295$ K: fluorescence experiments (circles), Stokes−Einstein calculation (open diamond), MD trajectory (filled diamond) and NMR experiments corresponding to $S^2 = 0.9$ (filled square) and $0.65 < S^2 < 1$ (open square, data taken from Figure 5).

However, while the results show very good agreement between the τ_R values obtained from the theoretical calculations and the fluorescence experiments, the NMR experiments yielded significantly higher values, with an important uncertainty, reflecting the possible presence of a certain amount of polymerized BHP in the solution. Two arguments tend to support this assumption. First, the NMR experiments were carried out on high concentration solutions (10 mM), which was the maximum limit before aggregation. This concentration was necessary to improve the signal of the ^{13}C relaxation in conditions of natural abundance of this isotope. By comparison, fluorescence experiments were made on 50 μM solutions of BHP, because the measurements would not be feasible at 10 mM, owing to the optical density of the NMR sample. Second, the NMR relaxation rates (Table 1) show the presence of a long time scale exchange process that concerns both the porphyrin and the handle phenyls, and cannot be explained by any of the internal motions of the molecule that range on a too short time scale (<120 ps). Therefore, this can only reflect intermolecular exchange and is likely due to aggregation.

Thus, the over-evaluated rotational correlation time observed by NMR may be an average of an undetermined distribution of τ_R values corresponding to different associations of 1, 2, or more BHP molecules.

2. Internal Flexibility. The NMR relaxation experiments of an intermediary size system as BHP provides little insights into the internal dynamics due to the very low number of unequivalent $^1H-^{13}C$ vectors available. In our case, because of the molecule symmetry, the NMR experiments permitted the determination of relaxation parameters for only two sites: the eight C−H vectors of the porphyrin which are equivalent and the eight C−H vectors of the handle phenyls (four for each phenyl: the distal and the proximal ones) which are also equivalent. In these conditions, MD simulations are a useful complementary tool necessary to obtain a more complex internal dynamics description.

In NMR experiments, the longitudinal rate constants, R_1, for porphyrin and handle phenyls are significantly different (3.5 s^{-1} for the former and 1.9 s^{-1} for the latter), indicating that the internal motion of the phenyls may be less restrained than that of the porphyrin. This information was clearly corroborated by the atomic fluctuations calculated from the MD trajectory (Figure 4), as well as by the order parameters deduced from the rate constants ($0.65 \leq S^{2\,\mathrm{NMR}}_{porp} \leq 1$ and $0 \leq S^{2\,\mathrm{NMR}}_{phe} \leq 0.6$) despite their large uncertainty. The order parameters calculated from the MD simulations are within the intervals obtained from NMR ($S^{2\,\mathrm{MD}}_{porp} = 0.9$ and $S^{2\,\mathrm{MD}}_{phe} = 0.09$ and 0.13 for the proximal and distal phenyls, respectively).

3. MD and NMR Internal Dynamics Comparison. Despite the good evaluation of the S^2 order parameters, the (S^2,τ) couples obtained from MD simulations appear to be underestimated when compared to the NMR results for both the porphyrin and the handle phenyls, yielding small values for calculated relaxation rates. However, at least considering the τ_R values, it seems that, as mentioned above, the NMR experiments gave an overestimated rotational correlation time and, thus, a larger value for the porphyrin's relaxation rates.

3.1. Porphyrin Relaxation Rates. The calculation of the porphyrin relaxation rates using the Lipari−Szabo model with parameters obtained from the MD trajectory ($S^2 = 0.9$, $\tau_R = 119.5$ ps and $\tau_e = 0.1$ ps) yields $R^{MD}_{1_{porp}} \simeq R^{MD}_{2_{porp}} \simeq 2.3\ s^{-1}$ (Table 2), which is significantly smaller than the experimental results $\sim 3.5\ s^{-1}$ (Table 1, where the exchange contribution to R_2 is omitted). These calculated values correspond to temperature (302 K) higher than that of NMR experiments (295 K). Thus, to be comparable, the relaxation rates were calculated again, using τ^{MD}_R at 295 K, i.e., $\tau_R = 132.6$ ps (S^2 and τ_e were considered not to change significantly in this range of temperature). The results $R^{MD}_{1_{porp}} \simeq R^{MD}_{2_{porp}} \simeq 2.5\ s^{-1}$ are still smaller than what is observed experimentally. In fact to obtain the experimental results, τ_R should be equal to 206 ps, which is the average correlation time that corresponds to $S^2 = 0.9$ in Figure 5. As explained above, this discrepancy reflects most probably an over-estimation of the NMR relaxation rates due to the presence of a certain amount of polymerized BHP in the solution.

3.2. Handle-Phenyls Relaxation Rates. The handle-phenyls relaxation rates were calculated using the Clore−Szabo model and, as for the porphyrin, the internal correlation times and order parameters were not changed with respect to temperature. Comparison of experimental and computational values at 295 K, i.e., for $\tau_R = 132.6$ ps, shows that the latter ($R^{MD}_{1_{phe}} \simeq R^{MD}_{2_{phe}} \simeq 1.0\ s^{-1}$, Table 2) are effectively smaller than the former ($\approx 1.9\ s^{-1}$, Table 1). Notice that for the porphyrin, the polymerization had the effect of increasing the apparent τ_R value to 209 ps. Thus, the phenyls' relaxation rates were calculated again using this τ_R value, but the results were still significantly smaller than experimental ones $R^{MD}_{1_{phe}} \simeq R^{MD}_{2_{phe}} \simeq 1.2\ s^{-1}$, showing that the discrepancy is not only due to the mechanical slow of the molecule's overall tumbling. Even for the highest value of τ_R that could be reached from the contour plots in Figure 5 ($\tau_R = 340$ ps), the relaxation rates ($R^{MD}_{1_{phe}} \simeq R^{MD}_{2_{phe}} \simeq 1.5\ s^{-1}$) are still smaller than experimental values, although the corresponding porphyrin's relaxation rates ($R^{MD}_{porp}(\tau_R = 340\ \mathrm{ps}) \simeq 5\ s^{-1}$) are higher than what is observed experimentally. This can have at least two explanations: first, the effect of polymerization on the rotational correlation time was taken into account, but not that on the internal dynamics of the handle phenyls, which would be hindered if two molecules or more are associated together. Thus, in NMR experiments the S^2 order parameters could be higher than what they should be for a single molecule. Second, the problem can be due to the force field used in MD simulations, which can be responsible for a possible artifactual speeding up of the handle-phenyls movement. As seen before, this movement can be divided into three types: the handle bending, the phenyl sliding and the phenyl rotation. The handle bending is mainly governed by the rotation of the *meso*-phenyl around the bond relating it to the porphyrin. The force constant corresponding to this dihedral angle was based on quantum mechanical calculations[33] and can be considered a priori as reliable. The phenyl sliding is governed by the motion of all

the atoms of the handle except the phenyl itself. The parameters used to describe these motions were taken from Hayward et al.[31] and Smith and Karplus[32] and can also be considered as reliable, contrarily to the parameters used to describe the phenyl's rotation around its axis. Indeed the force constant used for the dihedral angles that correspond to the phenyl's rotation was taken by similarity from that of the cycle's rotation of phenylalanine residues in proteins; i.e., it was equal to zero. This might have sped up the phenyl's rotation and decreased the corresponding correlation time and consequently, the calculated relaxation rates.

Despite the possible speeding of the phenyl's rotation, this motion is still the slowest internal one in BHP, contrarily to what would be expected intuitively. Indeed the correlation time for the handle-phenyls rotation ranges between 39 and 82 ps, whereas the handle's bending and the phenyl's sliding motions are 1 order of magnitude faster (∼3−5 ps).

4. Comparison with Proteins. On the basis of MD simulations, Horita et al.[55] divided the N−H vectors motion in proteins into two classes: fast motion in rigid secondary structure elements (e.g., helices), showing a monoexponential correlation function, $C(t)$, that decays rapidly with a time constant $\tau_e \sim 0.04-0.1$ ps and $S^2 \sim 0.8-0.9$, and slow motion in flexible regions (e.g., loops) frequently showing a biexponential decay characterized by $S^2 \leq 0.6$ with time constants $\tau_{fast} \sim 0.04-0.1$ ps and $\tau_{slow} \geq 50$ ps. The results obtained here for BHP are in the same range except for the phenyl's τ_{fast}. Indeed, the rigid part of the molecule, i.e., the porphyrin was easily described by the Lipari−Szabo approximation, yielding $S^2 = 0.9$ and $\tau_e = 0.1$ ps, and the flexible part, i.e., the handle phenyls were described by the Clore−Szabo model yielding $S^2 = 0.09-0.13$, $\tau_{fast} = 3.3-5.3$ ps and $\tau_{slow} = 108-119$ ps.

Generally, in proteins, the calculated order parameters from MD simulations that correspond to flexible regions of the molecule are underestimated,[54,58] because of the bad convergence of the correlation function due to the shortness of the trajectory. In the case of BHP, the convergence was well-attained for both the porphyrin and the handle phenyls. This may explain the difference between the τ_{fast} value calculated for BHP and those given for proteins.

5. Structural Considerations. In many aspects the 10 ns trajectory was sufficiently long to have a good sampling of the conformational space. Indeed, not only have all the calculated correlation functions well converged but also the average structure of BHP over the whole trajectory corresponded to the expectation of the chemists who synthesized the molecule as to its general shape, i.e., the handles were perfectly perpendicular to the porphyrin's plane and perpendicular to each other, and the handle-phenyls cycles were over the iron atom. However, this structure is the least probable one as can be seen from the point-map projections of the phenyls centers on the mean porphyrin plane in Figure 8, although it corresponded to the average of the configurations. It could be thought that this is due to the free energy cost of desolvating the iron atom, the chloroform having some dipole moment. But this is not the case, because in more than 60% of the trajectory frames there is no chloroform molecule in the vicinity of the metal and of these "unsolvated" frames, less than 2% correspond to the phenyl (either distal or proximal) over the center of the porphyrin. In fact the low probability to find the handle-phenyl's center over the iron atom can be mainly attributed to the presence of two amide groups in the anchor regions of the handle (Figure 1A) that restrain its internal motions. Indeed the presence of these groups reduces the motion of the handle to that of three planes,

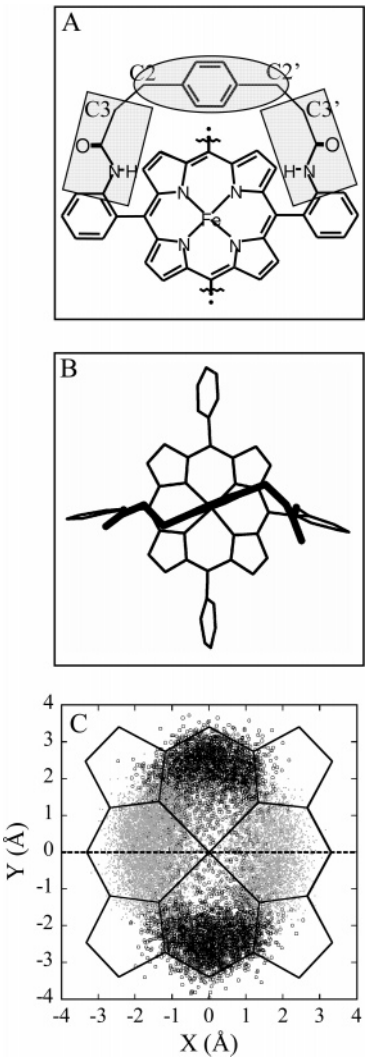

Figure 13. (A) 2D representation of BHP, with only one handle presented. The planes corresponding to the amide groups and the phenyl are shown. They are only connected by the bonds between atoms C2 and C3 on one hand and C2′ and C3′ on the other hand. (B) One representative frame from the MD trajectory corresponding to a conformation with the distal handle-phenyl's center over the metal. It is clearly seen that the handle (thick line) adopts an S conformation and the phenyl is perpendicular to the porphyrin plane. (C) projections of the center of the distal handle phenyl on the porphyrin plane (point-map as in Figure 8) where are represented only the points corresponding to the S conformation (gray dots) and those corresponding to the phenyl perpendicular to the porphyrin (angle between 80° and 90°, black open circles). One can see that these two sets are almost exclusive except in the center of the macrocycle.

corresponding to the two amide groups and the phenyl, connected by one covalent bond as shown in Figure 13A. The consequence is that, to have the phenyl's center over the metal with an acceptable energy cost, the handle should adopt an S conformation (Figure 13B) with the phenyl really perpendicular to the prophyrin plane (with an angle between 80° and 90°). As can be seen in Figure 13C, in the case of the distal handle, the first condition is fulfilled for the displacement along the *X*-axis while the second condition corresponds to the displacement along the *Y*-axis. Thus, the probability of having both conditions fulfilled is small. For the proximal handle, the axes are inverted.

There is a main difference between the expected experimental structure and the simulated average one: the out-of-plane dissymmetry of the porphyrin. Experimentally the Fe atom was

replaced by a tetracoordinated Zn, whereas in MD simulations the force field corresponded to that of a pentacoordinated Fe and a domed porphyrin, which introduced significant dissymmetry in the dynamical behavior of the distal and proximal handles. This difference was chosen for several reasons. First, the shape of a tetracoordinate Zn−porphyrin depends on the substituents of the macrocycle and this shape is not known in the case of ZnBHP. Second, since our main purpose was to study the behavior of the basket handles and how they encumber (or not) the vicinity of the metal (Fe or Zn), it was interesting to use a pentacoordinated iron in our simulations, so that on one side (distal) the handle phenyl was as far as possible from the metal and on the other side (proximal) the handle phenyl was as close as possible to the metal. In this way we explored the two extreme possibilities of the handle motions due to the out-of-plane position of the metal. It was observed that, despite some differences in the histograms (Figures 9 and 10), the qualitative behavior was similar (i.e., both handle phenyls avoid the position over the metal) as well as the internal correlation times of the handles and their phenyls (distal handle, $\tau_{fast} = 5.35 \pm 0.05$ ps and $\tau_{slow} = 119 \pm 2.1$ ps; proximal handle, $\tau_{fast} = 3.3 \pm 0.2$ ps and $\tau_{slow} = 108.5 \pm 9.7$ ps).

As cited in the Introduction section, BHP was synthesized with the aim of introducing a strong steric hindrance around the iron atom, due to the handle phenyls, that were expected to be parallel to the porphyrin plane and close to Fe. But the results presented in Figure 1B showed that the reaction rate (k_{on}) for binding CO and O_2 on BHP models was insensitive to the putative hindrance of the distal handle,[18,19,21,22] even in the case of the molecule studied here, that had the smallest and most rigid handle and was therefore expected to be the most encumbered on its distal side in its unliganded state. On the basis of the present study, this rather puzzling observation may be explained by the fact that the expected structure, where the handle phenyls are parallel to the porphyrin plane, was in fact highly improbable; the phenyls were actually found to lie rather perpendicular to the porphyrin plane along the whole trajectory. In addition, the handles and the phenyls were much more likely to be found most of the time displaced away from the porphyrin's normal passing through the Fe atom, making the effective steric hindrance considerably less than expected, despite the comparatively small size of the handles. Notice that this result does not provide any explanation about the "normal" behavior of the k_{off} rate. In that case the dynamics of the handles should be different from what is described here, not because of the pentacoordinate (domed) conformation of the liganded porphyrin (here the porphyrin is domed) but probably because of the interaction between the ligand and the distal handle. Naturally, this hypothesis cannot be verified without the presence of the ligand.

Conclusion

There were two aims for the present work, one was to give an explanation to the unusual behavior of the k_{on} rate in the LFER and the other was to investigate a medium-sized molecule for which available experimental data permit a meaningful test of the predictive power of MD in chemistry. The results show once more the complementarity between experiments and theoretical simulations, as well as the necessity to use both approaches jointly. The combination of fluorescence with MD simulations predicted well the global rotational correlation time (τ_R), but also suggested the possibility of some amount of aggregation of BHP in the NMR experiments accounting for the exchange part. NMR experiments gave qualitative information on the internal dynamics of the molecule while MD simulations permitted one to investigate the internal motions in more detail. Moreover, MD revealed some counterintuitive features regarding the time-averaged structure and its intrinsic low probability, which provided an explanation to the LFER observation. Finally, despite some bias introduced in the NMR measurements by a small amount of aggregation of BHP in concentrated solutions, MD simulations reproduced rather satisfactorily the relaxation rate constants observed by NMR and were able to predict at least semiquantitatively, the internal correlation times (τ_e, τ_{fast}, τ_{slow}). Therefore, it constituted a reliable technique to study average-sized systems where there are few experimental results with high uncertainties.

Acknowledgment. This work was supported by the Institut National de la Santé et de la Recherche Médicale (INSERM) and the Institut Curie. R.P. had grants from Gouvernement Français, Société de Secours des Amis des Sciences, Relations Internationales de l'Université Paris 6. The authors are indebted to Dr. Jeremy Smith, Dr. Chantal Houée-Levin, and Christiane Huel for their help and most of all to Dr. Daniel Lavalette who inspired and sustained this work.

References and Notes

(1) Tsuchida, E.; Komatsu, T. *Synthetic hemes*; 1994; Vol. 231.
(2) Momenteau, M.; Reed, C. *Chem. Rev.* **1994**, *94*, 659−698.
(3) Collman, J. P.; Eberspacher, T.; Fu, L.; Herrmann, P. C. *J. Mol. Catal. A* **1997**, *117*, 9−20.
(4) Slebodnick, C.; Ibers, J. A. *JBIC* **1997**, *2*, 521−525.
(5) Liang, H.; Dahan, M.; Karlin, K. D. *Curr. Opin. Struct. Biol.* **1999**, *3*, 168−175.
(6) Scheidt, W. R.; Ellison, M. K. *Acc. Chem. Res.* **1999**, *32*, 350−359.
(7) Wyllie, G. R. A.; Scheidt, W. R. *Chem. Rev.* **2002**, *102*, 1067−1089.
(8) Tani, F.; Matsu-ura, M.; Nakayama, S.; Naruta, Y. *Coord. Chem. Rev.* **2002**, *226*, 219−226.
(9) Zhang, Y.; Gossman, W.; Oldfield, E. *J. Am. Chem. Soc.* **2003**, *125*, 16387−16396.
(10) Collman, J. P.; Gagne, R.; Halbert, T. R.; Marchon, J. C.; Reed, C. A. *J. Am. Chem. Soc.* **1973**, *95*, 7868−7870.
(11) Wuenschell, G. E.; C.; T.; Lavalette, D.; Reed, C. *J. Am. Chem. Soc.* **1992**, *114*, 3346−3355.
(12) Collman, J. P.; Fu, L. *Acc. Chem. Res.* **1999**, *32*, 455−463.
(13) Momenteau, M.; Look, B.; Mispelter, J.; Bisagni, E. *Nouv. J. Chim.* **1979**, *3*, 77.
(14) Momenteau, M.; Look, B. *J. Mol. Catal.* **1980**, *7*, 315.
(15) Jimenez, H. R.; Moratal, J. M.; Faus, J.; Momenteau, M. *New J. Chem.* **1994**, *18*, 1247−1252.
(16) Landergren, M.; Baltzer, L. *J. Chem. Soc., Perkin Trans. 2* **1992**, *2*, 355−359.
(17) Momenteau, M.; Lavalette, D. *J. Chem. Soc., Chem. Commun.* **1982**, 341−343.
(18) Tetreau, C.; Lavalette, D.; Momenteau, M.; Lhoste, J. M. *Proc. Natl. Acad Sci. U.S.A.* **1987**, *84*, 2267−2271.
(19) Tetreau, C.; Momenteau, M.; Lavalette, D. *Inorg. Chem.* **1990**, *29*, 1727−1731.
(20) Lavalette, D.; Tetreau, C.; Mispelter, J.; Momenteau, M.; Lhoste, J. M. *Eur. J. Biochem.* **1984**, *145*, 545−565.
(21) Lavalette, D.; Tetreau, C.; Momenteau, M.; Mispelter, J.; Lhoste, J. M.; Wuenschell, G. E.; Reed, C. *Laser Chem.* **1990**, *10*, 297−318.
(22) Tetreau, C.; Lavalette, D.; Momenteau, M.; Fischer, J.; Weiss, R. *J. Am. Chem. Soc.* **1994**, *116*, 11840−11848.
(23) Momenteau, M.; Mispelter, J.; Loock, B.; Bisagni, E. *J. Chem. Soc., Perkin Trans. 1* **1983**, *I*, 189−196.
(24) Momenteau, M.; Mispelter, J.; Loock, B.; Lhoste, J.-M. *J. Chem. Soc., Perkin Trans. 1* **1985**, *1*, 61−70.
(25) Momenteau, M.; Mispelter, J.; Loock, B.; Lhoste, J. M. *J. Chem. Soc., Perkin Trans. 1* **1985**, *1*, 221−231.
(26) Momenteau, M.; Look, B.; Huel, C.; Lhoste, J. *J. Chem. Soc., Perkin Trans. 1* **1988**, 283−295.
(27) Collman, J. P.; Hoard, J. L.; Kim, N.; Lang, G.; Reed, C. *J. Am. Chem. Soc.* **1975**, *97*, 2676−2681.
(28) Collman, J. P.; Gagne, R. R.; Reed, C.; Halbert, T. R.; Lang, G.; Robinson, W. T. *J. Am. Chem. Soc.* **1975**, *97*, 1427−1439.
(29) Brünger, A.; Karplus, M. *Proteins* **1988**, *4*, 148−156.

(30) Brooks, B. R.; Bruccoleri, R. E.; Olafson, B. D.; States, D. J.; Swaminathan, S.; Karplus, M. *J. Comput. Chem.* **1983**, *4*, 187−217.
(31) Hayward, R. L.; Middendorf, H. D.; Wanderlingh, U.; Smith, J. C. *J. Chem. Phys.* **1995**, *102*.
(32) Smith, J. C.; Karplus, M. *J. Am. Chem. Soc.* **1992**, *114*, 801−812.
(33) Tsuzuki, S.; Tanabe, K. *J. Phys. Chem.* **1991**, *95*, 139−144.
(34) Frisch, M. J.; Trucks, G. W.; Schlegel, H. B.; Scuseria, G. E.; Robb, M. A.; Cheeseman, J. R.; Zakrzewski, V. G.; Montgomery, J. A., Jr., R. E. S.; Burant, J. C.; Dapprich, S.; Millam, J. M.; Daniels, A. D.; Kudin, K. N.; Strain, M. C.; Farkas, O.; Tomasi, J.; Barone, V.; Cossi, M.; Cammi, R.; Mennucci, B.; Pomelli, C.; Adamo, C.; Clifford, S.; Ochterski, J.; Petersson, G. A.; Ayala, P. Y.; Cui, Q.; Morokuma, K.; Salvador, P.; Dannenberg, J. J.; Malick, D. K.; Rabuck, A. D.; Raghavachari, K.; Foresman, J. B.; Cioslowski, J.; Ortiz, J. V.; Baboul, A. G.; Stefanov, B. B.; Liu, G.; Liashenko, A.; Piskorz, P.; Komaromi, I.; Gomperts, R.; Martin, R. L.; Fox, D. J.; Keith, T.; Al-Laham, M. A.; Peng, C. Y.; Nanayakkara, A.; Challacombe, M.; Gill, P. M. W.; Johnson, B.; Chen, W.; Wong, M. W.; Andres, J. L.; Gonzalez, C.; Head-Gordon, M.; Replogle, E. S.; Pople, J. A. Gaussian 98 ed.; Gaussian, Inc.: Pittsburgh, PA, 2001.
(35) Tironi, I. G.; Van Gunsteren, W. F. *Mol. Phys.* **1994**, *83*, 381−403.
(36) Ryckaert, J. P.; Cioccotti, G.; Berendsen, H. J. C. *J. Comput. Phys.* **1977**, *23*, 327−341.
(37) Verlet, L. *Phys. Rev.* **1967**, *159*, 98−103.
(38) Mispelter, J.; Lefevre, C.; Adjadj, E.; Quiniou, E.; Favaudon, V. *J. Biomol. NMR* **1995**, *5*, 233−244.
(39) Vincent, M.; Gallay, J.; Demchenko, A. P. *J. Phys. Chem.* **1995**, *99*, 14931−14941.
(40) Rouviere, N.; Vincent, M.; Craescu, C. T.; Gallay, J. *Biochemistry* **1997**, *36*, 7339−7352.
(41) Carrington, A.; MacLachlan, A. D. *Introduction to magnetic resonance with applications to chemistry and chemical physics*; Harper and Row: New York, 1967.
(42) Chandrasekhar, I.; Clore, G. M.; Szabo, A.; Gronenborn, A. M.; Brooks, B. R. *J. Mol. Biol.* **1992**, *226*, 239−250.
(43) Yamasaki, K.; Saito, M.; Oobatake, M.; Kanaya, S. *Biochemistry* **1995**, *34*, 6587−6601.
(44) Abragam, A. *The principles of nuclear magnetism*; Clarendon: Oxford, 1961.
(45) Orendt, A. M.; Sethi, A. K.; Facelli, J. C.; Horton, S. W. J.; Pugmire, R. J.; Grant, D. M. *J. Am. Chem. Soc.* **1992**, *114*, 2832−2836.
(46) Wang, W.; Phung, C. G.; Alderman, D. W.; Pugmire, R. J.; M.Grant, D. *J. Am. Chem. Soc.* **1995**, *117*, 11984−11988.
(47) Orendt, A. M.; Facelli, J. C.; Bai, S.; Rai, A.; Gossett, M.; Scott, L. T.; Boerio-Goates, J.; Pugmire, R. J.; Grant, D. M. *J. Phys. Chem. A* **2000**, *104*, 149−155.
(48) Barich, D. H.; Orendt, A. M.; Pugmire, R. J.; Grant, D. M. *J. Phys. Chem. A* **2000**, *104*, 8290−8295.
(49) Facelli, J. C.; Nakagawa, B. K.; Orendt, A. M.; Pugmire, R. J. *J. Phys. Chem. A* **2001**, *105*, 7468−7472.
(50) Lipari, G.; Szabo, A. *J. Am. Chem. Soc.* **1982**, *104*, 4546−4559.
(51) Clore, G.; M.; A.; S.; Bax, A.; Driscoll, P.; C.; Kay, L.; E.; Gronenborn, A.; M. *J. Am. Chem. Soc.* **1990**, *112*, 4989−4991.
(52) Jin, D.; Andrec, M.; Montelione, G. T.; Levy, R. M. *J. Biomol. NMR* **1998**, *12*, 471−492.
(53) Smith, P. E.; van Schaik, R. C.; Szyperski, T.; Wuthrich, K.; van Gunsteren, W. F. *J. Mol. Biol.* **1995**, *246*, 356−365.
(54) Pfeiffer, S.; Fushman, D.; Cowburn, D. *J. Am. Chem. Soc.* **2001**, *123*, 3021−3036.
(55) Horita, D. A.; Zhang, W.; Smithgall, T. E.; Gmeiner, W. H.; Byrd, R. A. *Protein Sci.* **2000**, *9*, 95−103.
(56) Weast, R. C., Ed. *CRC Handbook of Chemistry and Physics*, 52nd ed.; The Chemical Rubber Co.: Boca Raton, FL, 1971.
(57) Brüschweiler, R.; Roux, B.; Blackledge, M.; Karplus, M.; R.; E. R. *J. Am. Chem. Soc.* **1992**, *114*, 9−2302.
(58) Philippopoulos, M.; Lim, C. *J. Mol. Biol.* **1995**, *254*, 771−792.